ELSEVIER

Journal of Structural Geology 26 (2004) 2175–2189

JOURNAL OF STRUCTURAL GEOLOGY

www.elsevier.com/locate/jsg

Regional scale strain variations in Banded Iron Formations of Eastern India: results from anisotropy of magnetic susceptibility studies

A. Mukherji, A.K. Chaudhuri, M.A. Mamtani*

Department of Geology & Geophysics, Indian Institute of Technology, Kharagpur 721302, India

Received 9 December 2003; received in revised form 18 May 2004; accepted 31 May 2004

Available online 10 August 2004

Abstract

Anisotropy of magnetic susceptibility (AMS) data are used as a tool to determine strain variations in different parts of the Banded Iron Formations (BIFs) of the Bonai Synclinorium, eastern India. AMS data of 88 cylindrical cores drilled from 29 samples collected from the limb and hinge parts of mesoscopic scale folds as well as different parts of the entire synclinorium are presented. It is found that the samples from limbs of small-scale folds and also from limbs of the regional scale synclinorium have higher degrees of anisotropy than the hinges. This is inferred to indicate that the limbs accommodated higher strain than the hinges. AMS orientation data are analysed in conjunction with field data. It is concluded that the magnetic fabric developed in the limbs as well as hinges of the BIFs of the study area is related to deformation and is not a manifestation of sedimentary fabric.
© 2004 Elsevier Ltd. All rights reserved.

Keywords: Anisotropy of magnetic susceptibility; Banded Iron Formations; Strain; India

1. Introduction

Analysing strain in deformed rocks is an important aspect of structural geology studies. It involves determining the magnitude and direction of the strain ellipse or ellipsoid in two and three dimensions, respectively. Techniques such as the $R_f-\phi$ method, Fry method etc. are used to carry out strain analysis from field data (Ramsay and Huber, 1983). However, the above techniques require the presence of markers like deformed fossils, oolites, pebbles etc. In the absence of such markers, analysing strain, establishing variations in strain and strain gradients is a challenge. Recently, the anisotropy of magnetic susceptibility (AMS) data have been used for strain analysis in rocks that do not contain elliptical markers and there is a general consensus that the degree of magnetic anisotropy is a good indicator of strain magnitude (Hrouda, 1993; Tarling and Hrouda, 1993; Borradaile and Henry, 1997). AMS data have been used to analyse folds (e.g. Hrouda, 1978; Mamtani et al., 1999; Hrouda et al., 2000) and thrust tectonics (Jayangondaperumal and Dubey, 2001). Deformation studies using AMS data in rocks like granites that do not contain well-developed mesoscopic lineations and foliations have been extensively carried out (e.g. Bouchez et al., 1990; Archanjo et al., 1994; Cruden and Launeau, 1994; Leblanc et al., 1996; Bouchez, 1997; Djouadi et al., 1997; Ferré et al., 1997, 1999, 2002; Gleizes et al., 1997, 1998a,b, 2001; Saint-Blanquat and Tikoff, 1997; Benn et al., 1998, 1999; Siegesmund and Becker, 2000; de Wall et al., 2001; Greiling and Verma, 2001; Neves et al., 2003; Tomezzoli et al., 2003). Based on such AMS studies, variations in the magnitude of strain within granitic plutons have been noted and shear zones have been identified.

The present study deals with AMS studies on the Precambrian Banded Iron Formations (BIFs) of the Bonai Synclinorium, eastern India. Since the rocks do not preserve markers for using the conventional techniques for strain analysis, AMS data are used to analyse strain. Field as well as AMS data from rocks lying on the limb areas as well as the hinge areas of the synclinorium are presented. Regional-scale variations in the degree of magnetic anisotropy are recorded, which are inferred to be related to differences in strain conditions in different parts of the synclinorium. Magnetic data from limb and hinge parts of hand-specimen scale folds are also presented and the origin of the fabric (tectonic or depositional) is discussed. On the basis of the

* Corresponding author. Tel.: +91-3222-283388; fax: +91-3222-255303/282700.

E-mail address: mamtani@gg.iitkgp.ernet.in (M.A. Mamtani),

0191-8141/$ - see front matter © 2004 Elsevier Ltd. All rights reserved.
doi:10.1016/j.jsg.2004.05.003

study it is suggested that AMS is a useful tool to analyse strain and deformation fabrics in BIFs.

2. Regional geology

The Singhbhum Orissa Iron Ore Craton (SOIOC) extends over an area of approximately 40,000 km^2 in the eastern part of India. The study area is of the folded Archaean age Iron Ore Group (IOG) type. It comprises low-grade metasediments (BIFs) including phyllites, tuffaceous shales, banded hematite jaspers/banded hematite quartzites (BHJ/BHQ), with iron ore deposited on a metamorphic basement within the craton. The main regional structure influencing the IOG is a NNE-trending, low-plunging synclinorium overturned towards the east. The BIFs define a horseshoe shaped structure (Fig. 1) termed the 'Bonai Synclinorium' with the BHJ/BHQ forming the backbone of the iron ore range (western arm of Synclinorium) stretching across the region in a NNE–SSW direction (Jones, 1934).

The SOIOC is bounded by the arcuate Singhbhum Shear Zone to the north and the Sukinda Thrust to the south (Saha et al., 1988). A long Precambrian history recorded within this crustal unit includes distinct orogenic episodes accompanied by granite emplacement over different phases. The studied area is a part of the major Iron Ore Basin, which developed within the craton after the emplacement of two early phases of Singhbhum Granite (~3.3 Ga). The IOG rocks were then deposited in this basin and several episodes of crustal thickening, sedimentation and magma injection preceded the Iron Ore orogeny, which folded the IOG rocks prior to 2.8 Ga (Saha, 1994).

3. Field data

For the purpose of the present investigation, six mines in the study area were selected. These were the Gua and Bolani (western limb), Khandadhar and Sakradih (hinge) and Noamundi and Joda (eastern limb) mines. Detailed structural mapping and data collection of planar and linear structural elements from these mines was undertaken (see Fig. 1 for location of mines). Since the rocks of the study area are BIFs, and dominantly comprise BHJ and BHQ, the lithology does not allow the development of any penetrative fabric like axial plane cleavage or schistosity. As a result, the planar fabric observed in the field is S_0. Therefore the geometry of the folds observed in the field exposures, and the nature (curved or planar) of the observable axial surface, was taken as the criteria for differentiating folds of different generations. A superposed fold history involving three phases of deformation, viz. D_1, D_2 and D_3, has been worked out.

D_1 deformation resulted in the development of folds that have a reclined to inclined geometry. The fold axis of D_1 folds trend in the NW–SE to N–S direction. Hinges of small-scale folds defining fold axis parallel lineations (L_1) that developed during D_1 have been measured at several places in the region and have similar orientations as the fold axis mentioned above. Moreover, although an axial plane schistosity/cleavage has not developed in these rocks because the lithology does not favour its development, the axial plane direction is measurable in the field and is designated as AP_1. The orientation of AP_1 varies from NW–SE to NE–SW. D_2 deformation led to the development of open to tight D_2 folds with the fold axis varying between N–S and NNE–SSW. In places, the D_2 folds are also overturned. The coaxial superposition of D_2 folds over D_1 has resulted in development of hook-shaped geometry or Type-3 interference patterns (Ramsay, 1967). Fig. 2a highlights the hook-shaped geometry in the BIFs of the study area. The axial plane of D_2 folds is AP_2. It is relatively planar and generally strikes in a N–S to NE–SW direction. D_2 resulted in coaxial folding of D_1 due to which AP_1 is curved (Fig. 2a). The fold axis lineations related to D_2 folds are designated L_2 and have orientations that are parallel to L_1, thus implying the coaxial nature of D_1 and D_2 folds. D_3 deformation followed D_2 and resulted in a cross folding with the D_3 fold axis trending E–W to WNW–ESE. The D_3 folds are very broad, open and generally have an upright geometry with the axial plane (AP_3) striking E–W to WNW–ESE. Mesoscopic evidence of D_3, such as development of culminations and depressions/dome-basin Type-1 interference pattern (Ramsay, 1967), are developed in certain places (Fig. 2b). However, the effect of D_3 is dominantly recorded from the variation in geometry of planar and linear structures of earlier generations.

A large database has been generated from detailed field studies on the limbs and hinge of the Bonai Synclinorium and these data were subjected to a rigorous structural analysis using lower hemisphere equal area projections, the details of which are beyond the scope of the present paper. Fig. 3 is a synoptic diagram that documents the results from this analysis. A critical examination of the equal area projections brings out the points that were discussed above. The effect of D_2 folds reorienting the D_1 fold structures is clear in Fig. 3a (Gua mine). The lineations related to earlier folds are observed to have been reoriented by D_3 folding in Fig. 3b (Gua mine). The dominance of D_2 folds is seen in Fig. 3c (Bolani mine). The variation in D_2 fold axes in Fig. 3d and e (both for Khandadhar mine) reflects the effect of D_3 on the D_2 fold axes. In Fig. 3f (Sakradih mine), the deformation was very heterogeneous and the effect of all the three deformations gives rise to a complex contoured diagram. Finally Fig. 3g and h (both from Joda mine) and Fig. 3i (Noamundi mine) show the effect of D_2 on D_1 deformation.

Besides the above, structural analysis of the field data also helps in deciphering the mechanism of folding of D_2 folds. It is observed that two distinct girdles are present for the poles of S_0 planes at Gua (Fig. 3a). One is the main girdle (shown in bold), which gives the orientation of β_1. The second one, the subordinate girdle (shown in dashes)

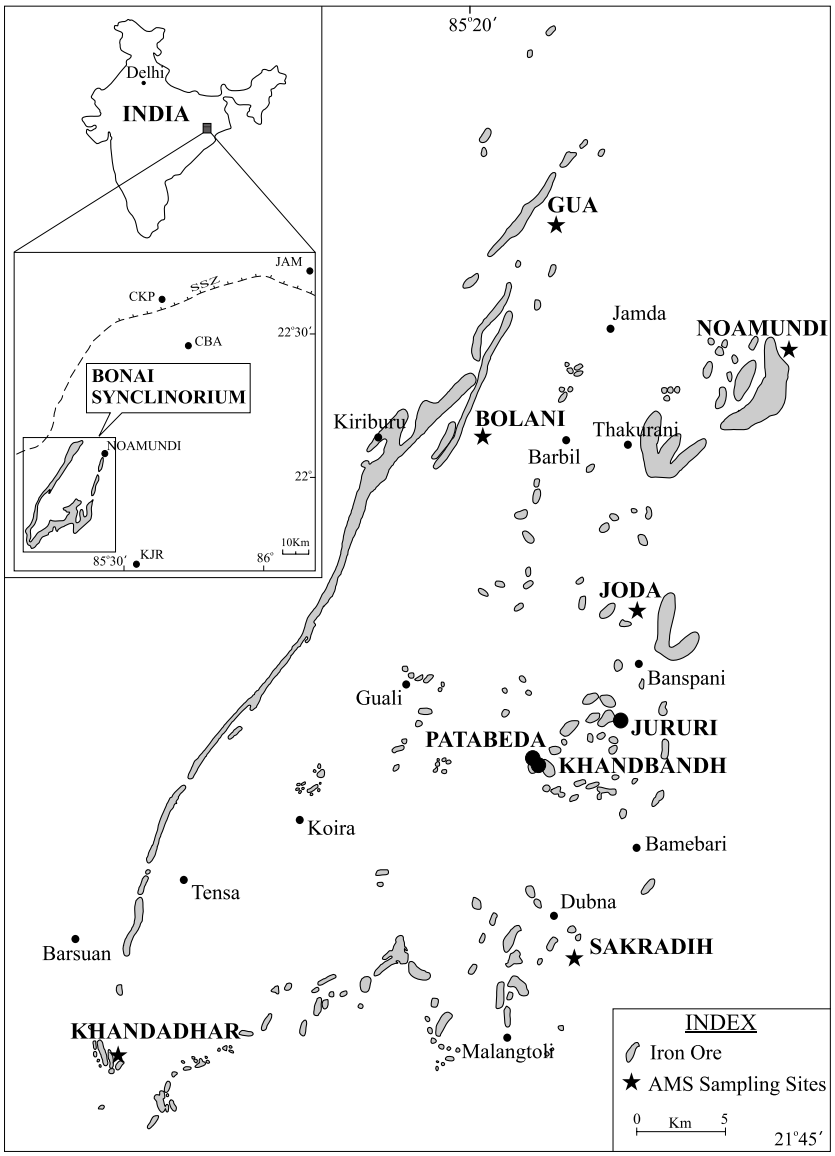

Fig. 1. Map of the Bonai Synclinorium within a part of the Singhbhum–Orissa craton in eastern India. The inset map shows the regional location (CKP—Chakradharpur; CBA—Chaibasa; JAM—Jamshedpur; KJR—Keonjhargarh; SSZ—Singhbhum Shear Zone).

gives the orientation of β_1'. Naha and Chaudhuri (1968) reported the presence of two similar girdles from the Precambrian rocks of the Aravalli Mountain Belt (north-western part of India) and referred to them as 'paired girdles'. They concluded that such a paired girdle pattern implies that flexural folding took place in the rocks due to which the subordinate β points rotated about the intersection of the paired girdles. Accordingly, it is inferred that the mechanism of D_2 folding in the BIFs of eastern India was of flexural type due to which the subordinate β_1' rotated about the intersection of the paired girdles.

4. AMS studies

The primary objective of this study was to determine the strain conditions in different parts of the synclinorium. As stated earlier, the BIFs do not contain any elliptical markers to allow strain analysis using conventional methods and, therefore, AMS studies were planned. This technique involves collection of oriented rock samples from the field, drilling cylindrical cores from them, followed by determination of the strength of magnetization that a sample acquires when an external magnetic field is applied in different orientations. Over the past few decades, AMS has been applied for strain analysis. The primary reasons for this are (a) the technique can be applied to any rock even in the absence of mesoscopic scale markers, (b) the analysis is fast and precise and gives 3D data, and (c) the problems with the interpretations with regard to strain magnitude are not significantly greater than for other methods (Tarling and Hrouda, 1993; Borradaile and Henry, 1997).

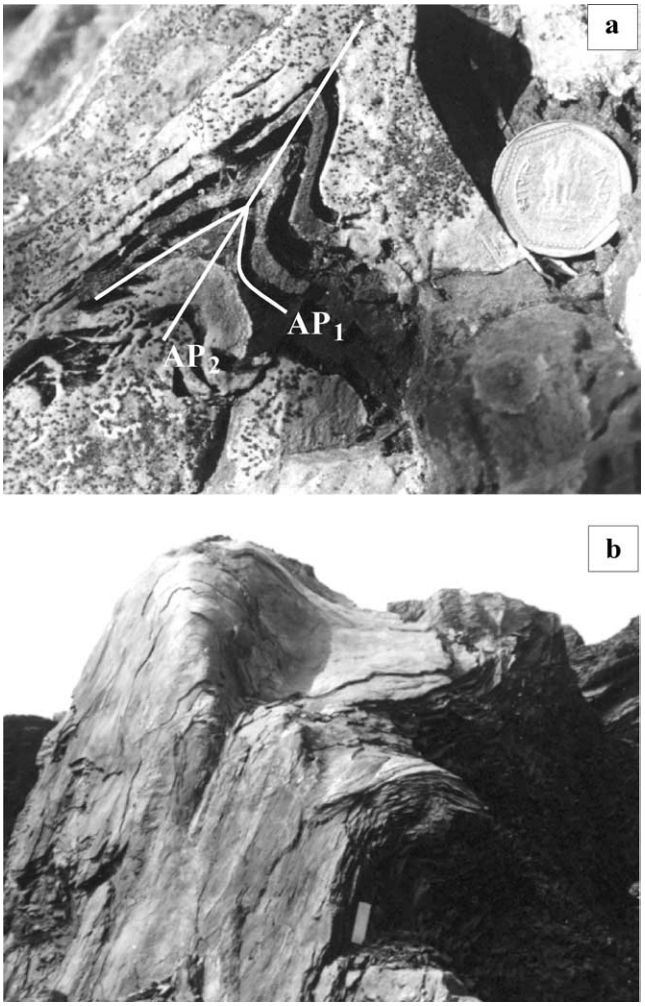

Fig. 2. (a) Small-scale hook (Type-3) interference pattern observed in BIFs of Patabeda mine. Camera faces N20°. (b) BIF outcrop within Khandadhar mine demonstrating culmination and depression developed due to superposition of D_3 folds on the D_2. Camera faces N185°.

AMS analysis gives the orientations and magnitudes of the three principal axes of the magnetic susceptibility ellipsoid, viz. K_1, K_2 and K_3, where $K_1 \geq K_2 \geq K_3$. For structural geology/tectonic interpretations, these three principal axes are equated with the three principal axes of the strain ellipsoid, X, Y and Z, respectively. There is a general consensus about the correlation between the principal directions of magnetic susceptibility and axes of the strain ellipsoid (Borradaile and Alford, 1987; Borradaile, 1988; Tarling and Hrouda, 1993; Borradaile and Henry, 1997). Although a similar correlation between the magnitude of the above two ellipsoids has been indicated by Rathore (1979), Rathore and Henry (1982) and Hrouda (1993), there has been a debate about whether it holds true because the AMS data are controlled by the mineralogy and magnetic behaviour of the dominant minerals, which may not be totally dependent on strain (Borradaile and Henry, 1997). However, it has been argued from experimental studies that a change in degree of magnetic anisotropy is related to the bulk strain ratio (Borradaile and Alford, 1987). Therefore, although the absolute values of the magnitude of the three axes of the susceptibility ellipsoid may not be correlatable with the magnitude of strain ellipsoid axes, AMS data are nevertheless a very useful measure of relative strain to establish strain gradients and note strain variations in rocks of similar/comparable lithology. Therefore, this method was suitable for carrying out strain analysis in the BIFs (BHJ/BHQ) of the study area.

4.1. Sampling and measurement

For AMS analysis, a total of 29 oriented rock samples of BHJ/BHQ and shale were collected from the field. Fig. 1 highlights the locations of the sampling sites. Care was taken to collect samples from the hinge (Khandadhar and Sakradih), western limb (Gua and Bolani) and eastern limb (Noamundi and Joda) of the horseshoe-shaped Bonai synclinorium in order to have a regional database from different parts of the synclinorium. With an aim to understand the nature of development of magnetic fabrics in different parts of mesoscopic folds and to visualise the regional scale strain variations, samples were also collected from limbs and hinge portions of small-scale folds in the field. Table 1 lists details of the samples collected from mesoscopic folds and their location (limb/hinge/between hinge and limb) on the fold. Cylindrical cores of 22 mm in height and 25.4 mm in diameter were drilled from each sample. For statistical treatment of AMS data, an attempt was made to drill multiple cores (2–3 cores) from each oriented sample. A total of 88 cylindrical cores were

Table 1
List of BIF samples collected from mesoscopic folds and their location (limb/hinge) on the fold surface

Name of mine	Sample no.	Core no.	Location on fold
Gua	GS-4	1	Limb
		2	Hinge
	GS-18	1	Hinge
		2	Hinge
		3	Between limb/hinge
		4,5,6	Limb
	GS-20	1	Hinge
	GS-23	2, 3	Limb
	GS-24	1,2,3,5	Limb
		4	Hinge
	SGU-2	1,2,3,4	Limb-1
	SGU-3	1,2,3	Limb-2
Bolani	BS-11	1.1,3	Limb
		1.2	Hinge
	SBO-8	1,2,4	Limb
Khandadhar	SKD-1	1,2,3	Limb-1
	SKD-2	1,2	Limb-2
Sakradih	SSK-1	1,2,3,4,5	Limb-1
	SSK-2	1,2,3	Limb-2
Noamundi	SNO-4	1,2,3,4,5,6	Limb-1
	SNO-5	1,2,3,4,5	Limb-2

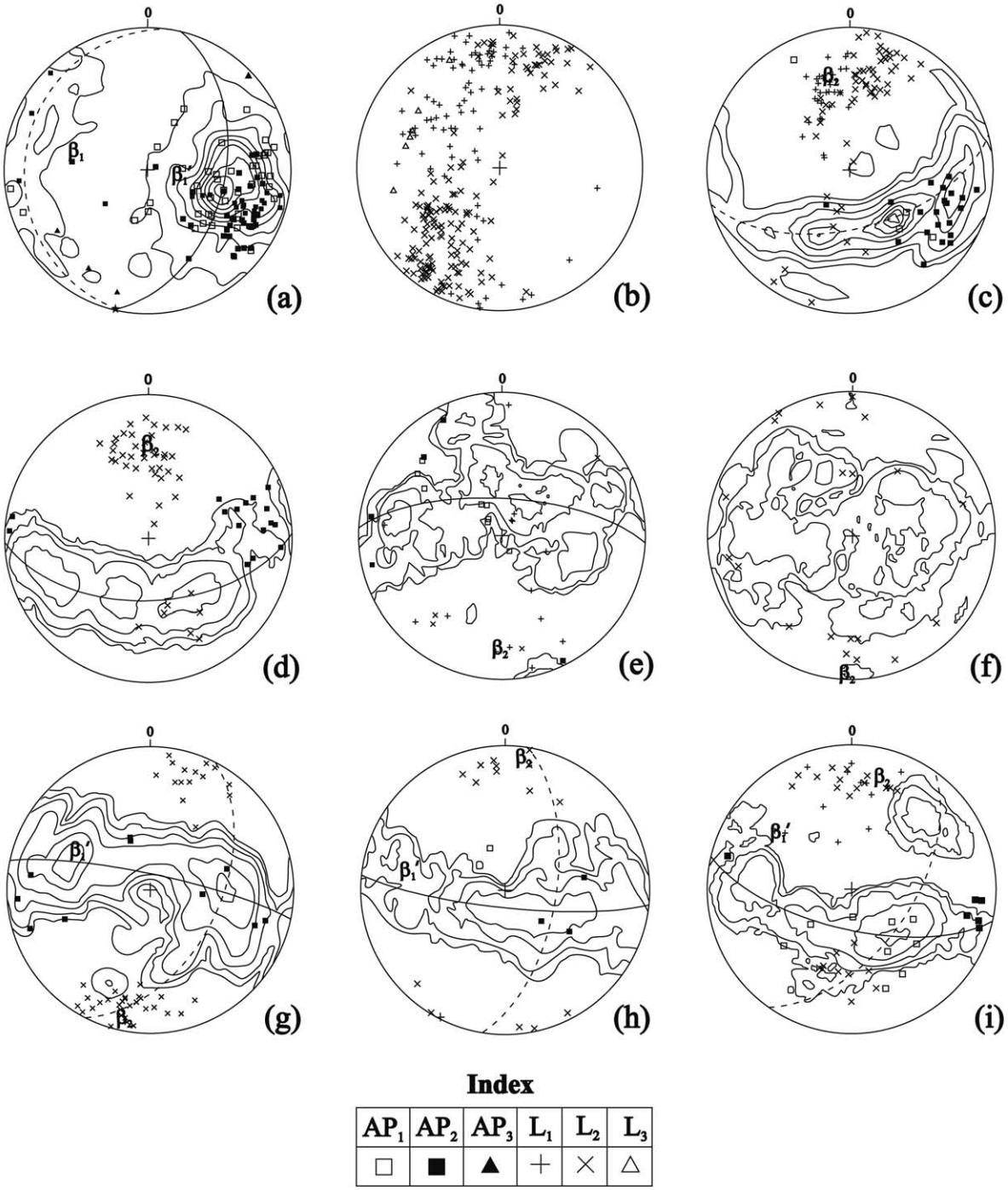

Fig. 3. Synoptic lower hemisphere equal area projections of the field planar and linear structural elements collected from different parts (mines) of the Bonai Synclinorium. In the figures β_1, β_2 and β_3 refer to fold axis orientation related to D_1, D_2 and D_3 deformation, respectively. (a) $n = 986$ S_0 poles from Gua; contours at 0.5, 1.5, 2.25, 3, 3.75, 4.5, 5.25, 6 and 6.75% per 1% area; $\beta_1 = 45°/285°$ and $\beta_1' = 75°/100°$. Intersection $\beta_2 = 02°/194°$; AP_1 ($n = 46$), AP_2 ($n = 58$) and AP_3 ($n = 4$). (b) Linear structures in Gua L_1 ($n = 86$), L_2 ($n = 157$) and L_3 ($n = 6$). (c) $n = 387$ S_0 poles from Bolani; contours at 0.5, 1, 2, 4, 6, 8, 10 and 11%, $\beta_1 = 34°/346°$. AP_1 ($n = 4$) and AP_2 ($n = 21$); lineations L_1 ($n = 32$) and L_2 ($n = 59$) are also plotted in the same diagram. (d) $n = 376$ S_0 poles from Khandadhar; contours at 1, 2, 4 and 8%; $\beta_2 = 36°/358°$; AP_2 ($n = 16$); lineation L_2 ($n = 46$). (e) $n = 122$ S_0 poles from a road cutting in Khandadhar; $\beta_2 = 21°/183°$ and contours are at 1, 2, 4 and 8% per 1% area; AP_1 ($n = 8$) and AP_2 ($n = 5$); lineations L_1 ($n = 14$) and L_2 ($n = 4$). (f) $n = 191$ S_0 poles from Sakradih; contours at 1, 2 and 4% and $\beta_2 = 05°/183°$; lineation L_2 ($n = 20$). (g) $n = 188$ S_0 poles from Joda; contours: 0.2, 0.5, 1, 2, 4 and 6%; $\beta_1' = 40°/297°$ and $\beta_2 = 09°/192°$; AP_2 ($n = 11$); lineation L_2 ($n = 44$). (h) $n = 208$ S_0 poles from a road cut in Joda; contours at 1, 2, 4 and 8% and $\beta_2 = 10°/006°$. Subordinate $\beta_1' = 29°/279°$; AP_1 ($n = 1$) and AP_2 ($n = 4$); lineations L_1 ($n = 1$) and L_2 ($n = 16$). (i) $n = 219$ S_0 poles from Noamundi; contours 1, 2, 4, 8 and 16%, $\beta_2 = 23°/13°$ and subordinate $\beta_1' = 34°/305°$; AP_1 ($n = 9$) and AP_2 ($n = 6$); lineations L_1 ($n = 13$) and L_2 ($n = 24$).

obtained from 29 oriented field samples and these were subjected to AMS analysis.

Measurement of magnetic susceptibility and its anisotropy was carried out using the KLY-3S Spinner Kappabridge manufactured by AGICO (Czech Republic) at the Wadia Institute of Himalayan Geology (Dehradun, India). The mean susceptibility (K_m) for each core and the magnitude and orientation of the three principal axes of the magnetic susceptibility ellipsoid, viz. K_1, K_2 and K_3, where $K_1 \geq K_2 \geq K_3$ were obtained along with other magnetic anisotropy parameters like anisotropy ratios, viz. magnetic foliation (F), magnetic lineation (L), corrected degree of anisotropy (P') and shape parameter (T) (Table 2). F and L are the magnitudes of the magnetic foliation and lineation, respectively. P' is a measure of the eccentricity of the magnetic susceptibility ellipsoid and T gives the shape of the susceptibility ellipsoid, i.e. prolate or oblate (Tarling and Hrouda, 1993).

4.2. AMS data

The mean bulk susceptibility (K_m) values in the samples vary from 64×10^{-6} to $236{,}500 \times 10^{-6}$ SI units. The lower values between 64.92×10^{-6} and 73.43×10^{-6} SI units were observed mainly in shales of Joda iron mine on the eastern limb of the Bonai Synclinorium. Low values between 724.3×10^{-6} and 2296×10^{-6} SI units are also found in some BIF samples from Khandadhar. The higher values between $115{,}400 \times 10^{-6}$ and $236{,}500 \times 10^{-6}$ SI units in general have been observed in samples of BIFs from Bolani and Gua.

The processing of the magnetic data involved preparation of Jelinek plots to investigate the type of strain that the rocks were subjected to (Tarling and Hrouda, 1993). A Jelinek plot (Fig. 4) comprises the corrected degree of anisotropy (P') on the X-axis and shape parameter (T) on the Y-axis. Separate plots were prepared for samples from different mines (Fig. 4). The plots showed that data from rocks of the study area fall dominantly in the oblate field indicating an oblate shape of the susceptibility ellipsoid.

The K_1, K_2 and K_3 orientation data were plotted as lower hemisphere equal area projections along with the field data (S_0) for that sample. As mentioned earlier, some of the samples were taken from different parts of mesoscopic scale folds, i.e. from the limb as well as hinge portions. Therefore, the AMS and field data from limbs (Fig. 5a) and hinges (Fig. 5b) of mesoscopic folds were plotted separately to understand the relation between location of samples on a folded surface, orientation of field structures and AMS fabric. It was observed that for samples from limbs of small-scale (mesoscopic scale) folds, the magnetic foliation is subparallel/parallel to the bedding plane (S_0). Conversely, there exists a moderate to high angle relationship between bedding plane (S_0) and magnetic foliation in samples from hinges of small-scale folds.

To analyse the regional scale variation in the degree of anisotropy (P') in different parts of the Bonai Synclinorium, a histogram of the average P' values calculated from all samples from each mine was prepared (Fig. 6). It was stated earlier that comparisons using AMS data are feasible only in cases of similar lithologies. Therefore, for the present purpose, BIF samples from the western limb (Gua and Bolani mines), eastern limb (Noamundi mines) and hinge (Khandadhar and Sakradih) of the Bonai Synclinorium were considered. Samples from Joda were not used for the present comparison since they are shales. It is clear from Fig. 6 that the P' values are higher in the samples from limbs than in those from the hinges.

5. Discussion

The above data are useful in providing information about the type of strain that was prevalent during deformation and folding of the BIFs of the study area. Fig. 4 clearly reveals that almost all the cores from different parts of the Bonai Synclinorium fall in the oblate field. This implies that the dominant strain in the region was of flattening type.

The variation in P' values in different parts of the synclinorium warrants a detailed discussion. Since the magnitudes of anisotropy and strain have been interpreted to be correlatable in earlier studies, the present authors also favour such an inference. The higher P' values in samples from the limbs and lower P' values for those from the hinge of the Bonai Synclinorium apparently indicate that the limbs were subjected to higher strain than the hinge. It is known from the work of Lister and Williams (1983) that limbs of folds accommodate higher strain than the hinges and, therefore, the above result of variation in P' values in different parts of the synclinorium supports this. However, caution needs to be exercised while making such an inference because the rocks of the study area are BIFs and AMS studies reveal that most of the BIF samples have high mean susceptibilities ($K_m > 1000 \times 10^{-6}$ SI units) and many have very high values with $K_m > 10{,}000 \times 10^{-6}$ SI units. This implies that ferromagnetic minerals like magnetite must be present in the rocks and these are responsible for the high susceptibilities in them. Mallik et al. (1993) and Das et al. (1996) reported the presence of multidomain (MD) magnetite from these rocks. Therefore, there is no doubt that magnetite is an important mineral that contributes to the high susceptibility of rocks of the study area. Moreover, the P' value also depends on the K_m of the sample, which is controlled by the volume percentage of ferromagnetic minerals present in the rock. Fig. 7 is a graph of the P' vs. K_m for samples of the study area. This gives an indication that the P' values could have also been controlled by the percentage of ferromagnetic minerals present in the rock rather then only by strain. To address this problem, the authors have analysed the samples taken from individual mesoscopic folds independently to observe the variation in P' values of cores from limb and hinge of each fold. Fig. 8a

Table 2
AMS data from rocks of the BIFs of the Bonai Synclinorium, Eastern India. (K_m = mean magnetic susceptibility in 10^{-6} SI units; F = magnetic foliation; L = magnetic lineation; P' = corrected degree of anisotropy; T = shape parameter; K_1, K_2 and K_3 represent magnitudes of maximum, intermediate and minimum axis of the magnetic ellipsoid, respectively; *D*/*I* represents the direction and amount of dip of principal axes of magnetic ellipsoid (in degrees))

	Sample no.	Core no.	K_m	F	L	P'	T	K_1	K_2	K_3	K_1 − *D*/*I*	K_3 − *D*/*I*
GUA	GS-1	1	10510	1.062	1.009	1.079	0.734	1.0262	1.0167	0.9571	276/40	118/48
	GS-1	2	9760	1.060	1.008	1.075	0.756	1.0246	1.0163	0.9591	268/37	122/48
	GS-1	3	10810	1.065	1.009	1.082	0.747	1.0269	1.0176	0.9556	278/40	122/47
	GS-1	4	12330	1.066	1.010	1.084	0.729	1.0280	1.0177	0.9544	271/39	121/47
	GS-1	5	11130	1.054	1.008	1.069	0.735	1.0229	1.0147	0.9624	271/33	120/54
	GS-3	1	13900	1.051	1.011	1.067	0.645	1.0236	1.0127	0.9637	020/60	237/25
	GS-3	2	10740	1.076	1.006	1.092	0.847	1.0282	1.0219	0.9499	359/47	237/26
	GS-3	3.1	9810	1.047	1.004	1.056	0.855	1.0175	1.0139	0.9686	008/55	244/21
	GS-3	3.2	7410	1.062	1.006	1.075	0.830	1.0234	1.0178	0.9588	345/01	255/19
	GS-4	1	119900	1.148	1.024	1.191	0.704	1.0613	1.0362	0.9025	207/29	085/44
	GS-4	2	61510	1.018	1.073	1.098	−0.596	1.0536	0.9819	0.9645	210/14	335/66
	GS-18	1	38560	1.063	1.053	1.119	0.089	1.0550	1.0023	0.9428	006/53	116/14
	GS-18	2	14710	1.030	1.025	1.056	0.101	1.0264	1.0016	0.9720	359/52	134/29
	GS-18	3	5344	1.015	1.005	1.020	0.506	1.0080	1.0032	0.9888	356/51	102/13
	GS-18	4	8787	1.002	1.022	1.026	−0.848	1.0151	0.9933	0.9916	357/53	122/23
	GS-18	5	12340	1.037	1.028	1.067	0.137	1.0308	1.0026	0.9666	336/55	169/34
	GS-18	6	15440	1.050	1.043	1.095	0.070	1.0444	1.0014	0.9542	353/51	140/34
	GS-20	1	3468	1.034	1.016	1.052	0.348	1.0221	1.0056	0.9723	053/50	207/37
	GS-23	2	92400	1.122	1.108	1.243	0.06	1.108	1.0004	0.8915	213/04	117/56
	GS-23	3	101000	1.130	1.015	1.162	0.787	1.0498	1.0347	0.9155	029/03	124/63
	GS-24	1	10000	1.022	1.007	1.030	0.502	1.0118	1.0047	0.9835	267/32	087/58
	GS-24	2	5529	1.005	1.006	1.011	−0.069	1.0054	0.9997	0.9948	013/55	248/22
	GS-24	3	4023	1.005	1.002	1.008	0.517	1.0030	1.0012	0.9958	012/39	257/27
	GS-24	4	3492	1.008	1.002	1.011	0.689	1.0038	1.0022	0.9940	169/83	263/00
	GS-24	5	7376	1.039	1.002	1.047	0.914	1.0139	1.0122	0.9739	283/32	082/56
	SGU-2	1	68680	1.099	1.017	1.127	0.705	1.0422	1.0253	0.9326	323/24	225/18
	SGU-2	2	66490	1.099	1.027	1.136	0.564	1.0489	1.0217	0.9294	318/12	225/15
	SGU-2	3	68480	1.102	1.023	1.135	0.626	1.0468	1.0238	0.9294	325/29	228/12
	SGU-2	4	56350	1.109	1.018	1.141	0.703	1.0463	1.0275	0.9262	325/25	229/12
	SGU-3	1	79400	1.126	1.035	1.174	0.554	1.0619	1.0264	0.9117	216/29	081/52
	SGU-3	2	81880	1.115	1.039	1.165	0.481	1.0618	1.0219	0.9163	212/29	078/52
	SGU-3	3	115400	1.091	1.048	1.145	0.301	1.0602	1.0119	0.9279	214/30	076/53
Bolani	BS-11	1.1	188100	1.230	1.039	1.303	0.687	1.0932	1.0519	0.8549	350/16	255/18
	BS-11	1.2	221400	1.117	1.021	1.152	0.680	1.0505	1.0286	0.9210	344/17	238/42
	BS-11	3	236500	1.143	1.046	1.204	0.494	1.0744	1.0269	0.8987	359/16	265/16
	SBO-5	1	32270	1.117	1.005	1.14	0.915	1.0397	1.0345	0.9258	249/04	115/84
	SBO-5	2	39540	1.131	1.006	1.156	0.908	1.0441	1.0379	0.9180	267/09	124/79
	SBO-5	3	32620	1.172	1.002	1.203	0.975	1.0528	1.0507	0.8965	215/04	105/78
	SBO-5	4	21710	1.030	1.003	1.037	0.804	1.0121	1.0088	0.9791	245/09	107/78
	SBO-5	5	32320	1.162	1.002	1.191	0.979	1.0500	1.0483	0.9018	223/04	098/83
	SBO-5A	1	52950	1.025	1.007	1.033	0.561	1.0126	1.0057	0.9816	257/09	089/81
	SBO-5A	2	65870	1.044	1.007	1.055	0.724	1.0188	1.0119	0.9693	275/08	047/78
	SBO-6A	1	93210	1.094	1.01	1.116	0.793	1.0363	1.0257	0.938	272/69	102/21
	SBO-6A	2	131300	1.11	1.014	1.138	0.763	1.0437	1.0291	0.9272	269/64	108/24
	SBO-6A	3	85410	1.097	1.007	1.118	0.856	1.0352	1.0278	0.9369	262/63	103/26
	SBO-8	1	97940	1.055	1.023	1.082	0.407	1.0331	1.0099	0.9570	232/59	067/30
	SBO-8	2	129200	1.024	1.026	1.051	−0.043	1.0254	0.9991	0.9755	079/75	232/14
	SBO-8	3	120400	1.018	1.029	1.048	−0.233	1.0252	0.9962	0.9786	049/73	248/17
	SBO-8	4	124000	1.050	1.027	1.079	0.287	1.0342	1.0067	0.9590	105/69	209/06
Khandadhar	KS-1	1	1497	1.052	1.005	1.063	0.814	1.0201	1.0148	0.9651	344/30	111/46
	KS-1	2	1734	1.055	1.007	1.069	0.776	1.0223	1.0154	0.9623	344/28	104/44
	KS-1	3	1445	1.052	1.011	1.068	0.637	1.0243	1.0129	0.9629	348/28	109/43
	KS-1	4.1	1393	1.050	1.001	1.059	0.956	1.0170	1.0159	0.9672	232/29	115/40
	KS-1	4.2	724.3	1.022	1.010	1.033	0.366	1.0141	1.0038	0.9821	199/06	104/35
	SKD-1	1	2006	1.044	1.016	1.063	0.464	1.0249	1.0088	0.9663	164/75	265/03
	SKD-1	2	1926	1.039	1.016	1.057	0.414	1.0234	1.0073	0.9693	156/75	262/04
	SKD-1	3	2296	1.045	1.019	1.067	0.411	1.0271	1.0083	0.9646	163/80	262/01
	SKD-2	1	933.4	1.033	1.013	1.048	0.433	1.0197	1.0065	0.9739	000/54	155/34
	SKD-2	2	1255	1.037	1.011	1.051	0.539	1.0196	1.0084	0.972	329/53	149/37

(*continued on next page*)

Table 2 (*continued*)

	Sample no.	Core no.	K_m	F	L	P'	T	K_1	K_2	K_3	$K_1 - D/I$	$K_3 - D/I$
	SKD-2A	1	1026	1.053	1.010	1.068	0.670	1.0237	1.0134	0.9629	352/47	155/41
	SKD-2A	2	1160	1.050	1.012	1.067	0.593	1.0244	1.0118	0.9638	345/50	164/40
	SKD-2A	3	1133	1.046	1.009	1.059	0.659	1.0210	1.0116	0.9674	354/48	157/41
Sakradih	SSK-1	1	1929	1.018	1.025	1.044	−0.174	1.0225	0.9974	0.9801	147/37	264/31
	SSK-1	2	2114	1.014	1.015	1.030	−0.047	1.0148	0.9995	0.9857	158/50	262/12
	SSK-1	3	1922	1.024	1.012	1.037	0.317	1.0158	1.0036	0.9806	133/42	265/37
	SSK-1	4	2217	1.022	1.020	1.043	0.060	1.0205	1.0007	0.9788	163/15	255/07
	SSK-1	5	2024	1.023	1.025	1.049	−0.051	1.0244	0.9990	0.9766	168/15	261/08
	SSK-2	1	2422	1.025	1.017	1.043	0.211	1.0194	1.0028	0.9779	323/56	178/29
	SSK-2	2	2283	1.022	1.031	1.054	−0.164	1.0278	0.9969	0.9753	317/57	180/25
	SSK-2	3	2163	1.015	1.026	1.042	−0.259	1.0221	0.9964	0.9816	311/50	203/15
Joda	JS-13	1	73.43	1.035	1.003	1.043	0.824	1.0136	1.0102	0.9762	332/43	125/43
	JS-13	2	68.88	1.033	1.001	1.039	0.917	1.0118	1.0104	0.9778	332/48	128/39
	JS-13	3	72.21	1.036	1.010	1.049	0.555	1.0186	1.0083	0.9731	334/43	126/43
	JS-13	4	70.79	1.063	1.007	1.078	0.790	1.0251	1.0178	0.9571	283/39	131/47
	JS-13	5	64.92	1.171	1.085	1.275	0.320	1.1071	1.0208	0.8720	237/12	115/68
	JS-13	6	65.59	1.027	1.006	1.035	0.626	1.0129	1.0067	0.9804	349/39	128/43
	SJE-2	1	1033	1.006	1.003	1.009	0.26	1.0041	1.0008	0.9952	266/59	097/31
Noamundi	SNO-4	1	1658	1.038	1.005	1.047	0.775	1.0155	1.0107	0.9737	045/28	194/58
	SNO-4	2	1503	1.031	1.011	1.044	0.464	1.0177	1.0063	0.9760	044/25	195/62
	SNO-4	3	1732	1.031	1.005	1.039	0.702	1.0137	1.0083	0.9780	357/29	192/60
	SNO-4	4	1610	1.035	1.009	1.047	0.580	1.0177	1.0083	0.9740	047/32	201/55
	SNO-4	5	1778	1.028	1.007	1.037	0.609	1.0135	1.0068	0.9796	357/34	189/55
	SNO-4	6	1740	1.032	1.003	1.039	0.837	1.0123	1.0095	0.9782	026/34	185/54
	SNO-5	1	22500	1.174	1.024	1.222	0.747	1.0680	1.0435	0.8895	016/16	132/57
	SNO-5	2	14930	1.114	1.007	1.137	0.88	1.0399	1.0328	0.9273	011/15	131/61
	SNO-5	3	20380	1.232	1.022	1.290	0.814	1.0818	1.0589	0.8593	019/13	141/66
	SNO-5	4	20900	1.128	1.013	1.158	0.813	1.0478	1.0349	0.9173	237/05	139/60
	SNO-5	5	17060	1.217	1.035	1.283	0.703	1.0869	1.0503	0.8629	043/05	142/59

is a histogram for P' values in cores drilled from the limbs and hinge of a mesoscopic scale fold from Gua (Sample GS-4). All the cores have very high K_m values ($>60{,}000 \times 10^{-6}$ SI units; Table 2) and therefore it is logical to infer that the volume percentages of magnetic minerals in the cores are comparable. Despite this, the cores from the limbs have higher P' values than those from the hinge. Similarly, each of the other histograms in Fig. 8b–d are for P' values from the hinges and limbs of individual mesoscopic scale fold from samples GS-24 (Gua), BS-11 (Bolani) and SBO-8 (Bolani), respectively. The K_m values show ranges of 3000–10,000, 188,100–236,500 and 97,940–129,200 $\times 10^{-6}$ SI units for GS-24, BS-11 and SBO-8, respectively (Table 2). Thus, K_m for cores from the hinge and limb of a particular fold is not significantly different. However, in each case, the cores from the limbs have higher P' values than those from the hinges, which indicates the role of strain. The relationship between P' and strain has also been mathematically investigated by Hrouda (1993) for four models, viz. passive, ductile, line/plane and viscous. It has been found that strain increases with the increase in P' for all the models. Even for ferromagnetic minerals such as magnetite and hematite, this relationship has been found to hold true (Hrouda, 1993). Therefore, based on this discussion and the results obtained from the present investigation of the BIFs of eastern India, it is suggested that the role of strain in controlling the P' values cannot be ignored. It is concluded that the limbs of mesoscopic scale folds in different mines must have accommodated higher strain than the hinges as a result of which the degree of anisotropy is higher in the limbs than the hinges. The same inference can also be extended to the regional scale on the basis of Fig. 6, which shows a higher value of P' for samples from the limbs of the synclinorium than the hinge. It is therefore inferred that the limbs of the Bonai Synclinorium were subjected to a higher strain than the hinges.

The relationship between field data and orientation of magnetic foliation is also interesting (Fig. 5). It is observed that the orientation of pole (K_3) to the magnetic foliation (K_1–K_2 plane) is parallel to pole of the bedding plane S_0 in the samples from limbs of mesoscopic scale folds. However, there is a moderate to high angle relationship between the poles of S_0 and K_3 orientations in samples from hinges of mesoscopic folds. Hrouda et al. (2002) have shown a superimposition of tectonic fabric over sedimentary fabric in the sedimentary rocks of the Veporic Unit of the central Western Carpathians (Slovakia). These authors argued that a low P' value and parallelism between bedding plane and magnetic foliation indicates a depositional origin of magnetic fabric, while a high P' and moderate to very large angles between magnetic foliation and bedding plane indicates that the magnetic fabric is related to deformational effects. In the present study of BIFs of eastern India,

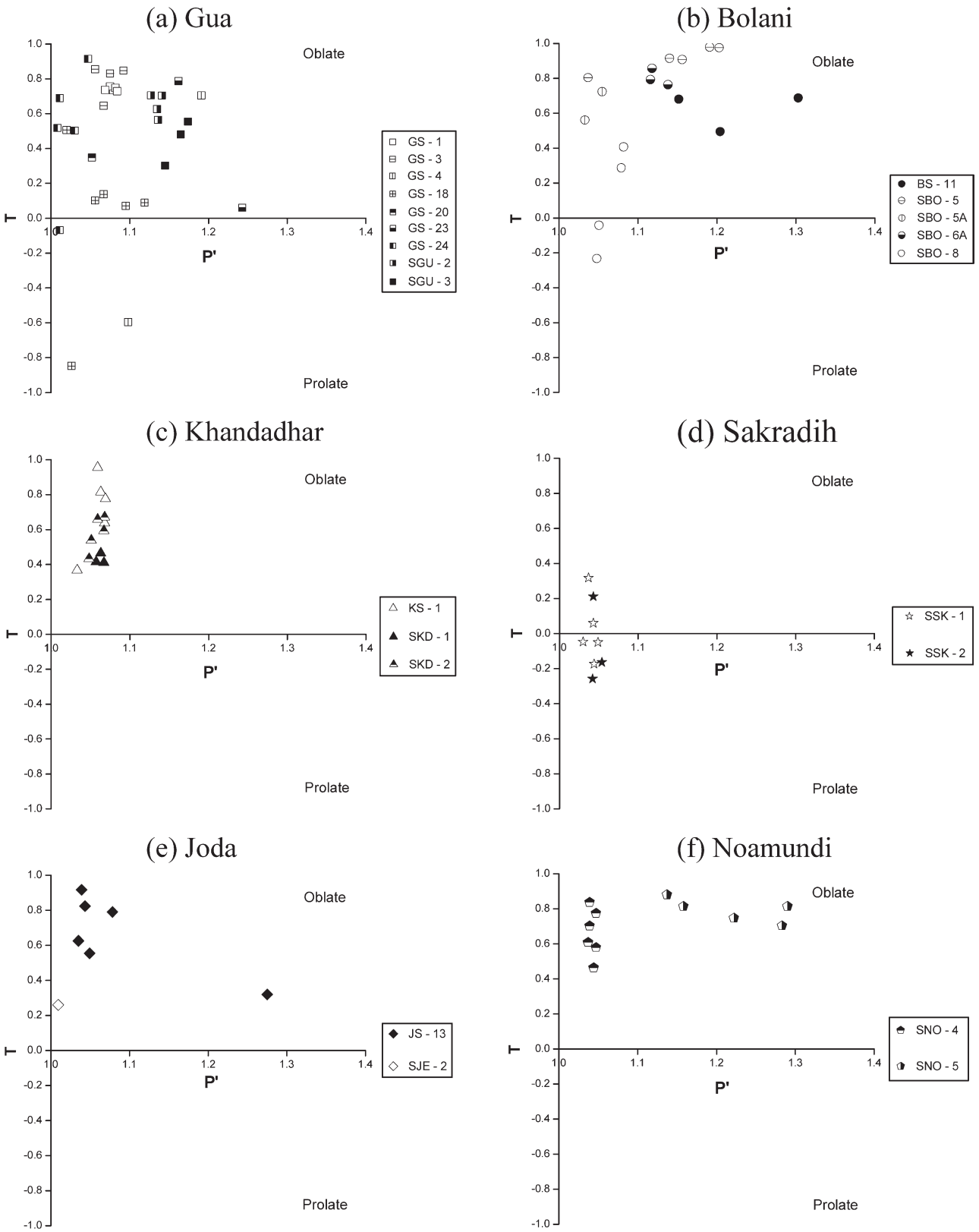

Fig. 4. Jelinek plots (P' vs. T) of magnetic data of BIF samples from (a) Gua, (b) Bolani, (c) Khandadhar, (d) Sakradih, (e) Joda and (f) Noamundi.

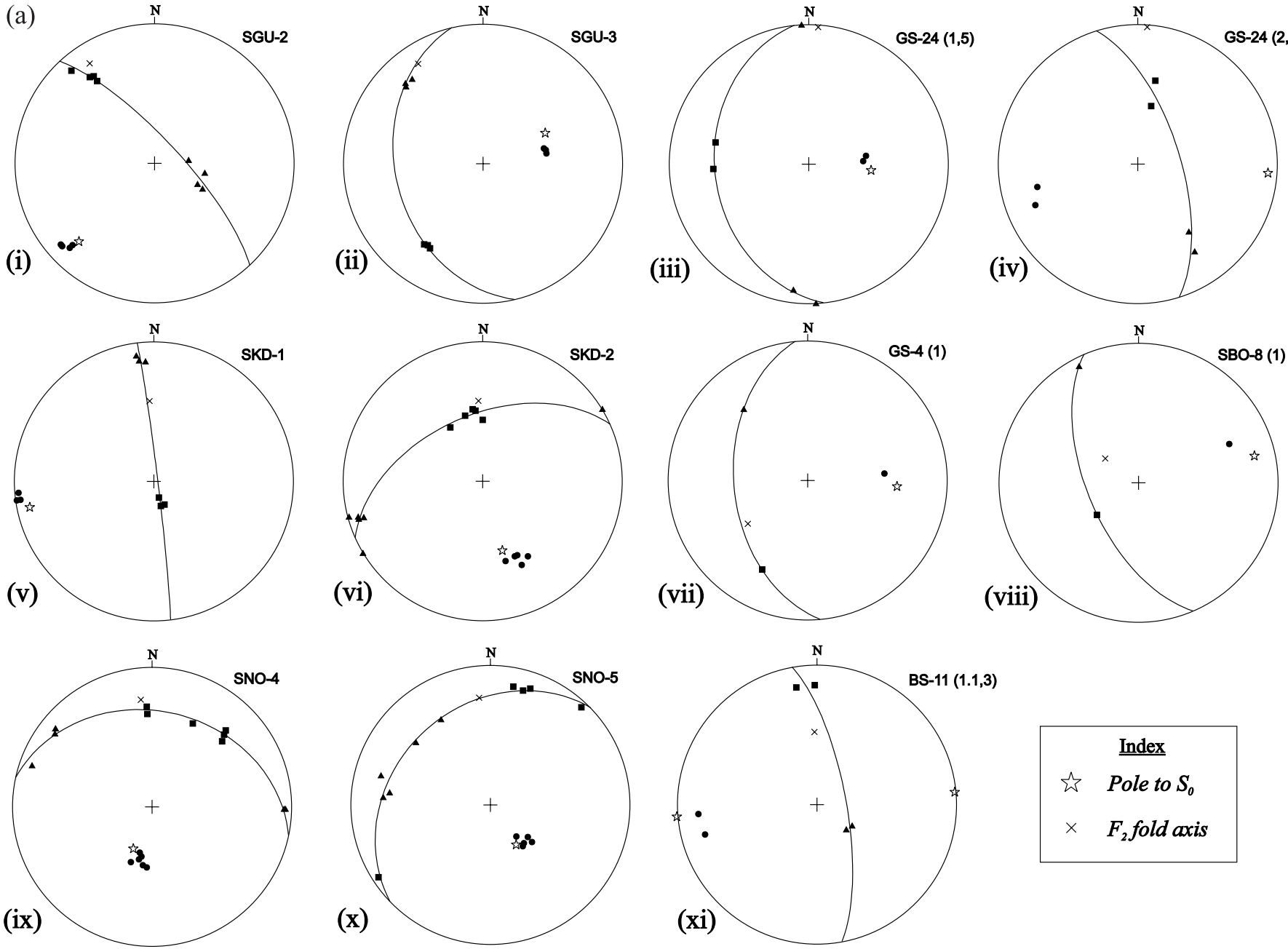
(a)
N
SGU-2
(i)
SGU-3
(ii)
GS-24 (1,5)
(iii)
GS-24 (2,3)
(iv)
SKD-1
(v)
SKD-2
(vi)
GS-4 (1)
(vii)
SBO-8 (1)
(viii)
SNO-4
(ix)
SNO-5
(x)
BS-11 (1.1,3)
(xi)
Index
Pole to S_0
F_2 fold axis

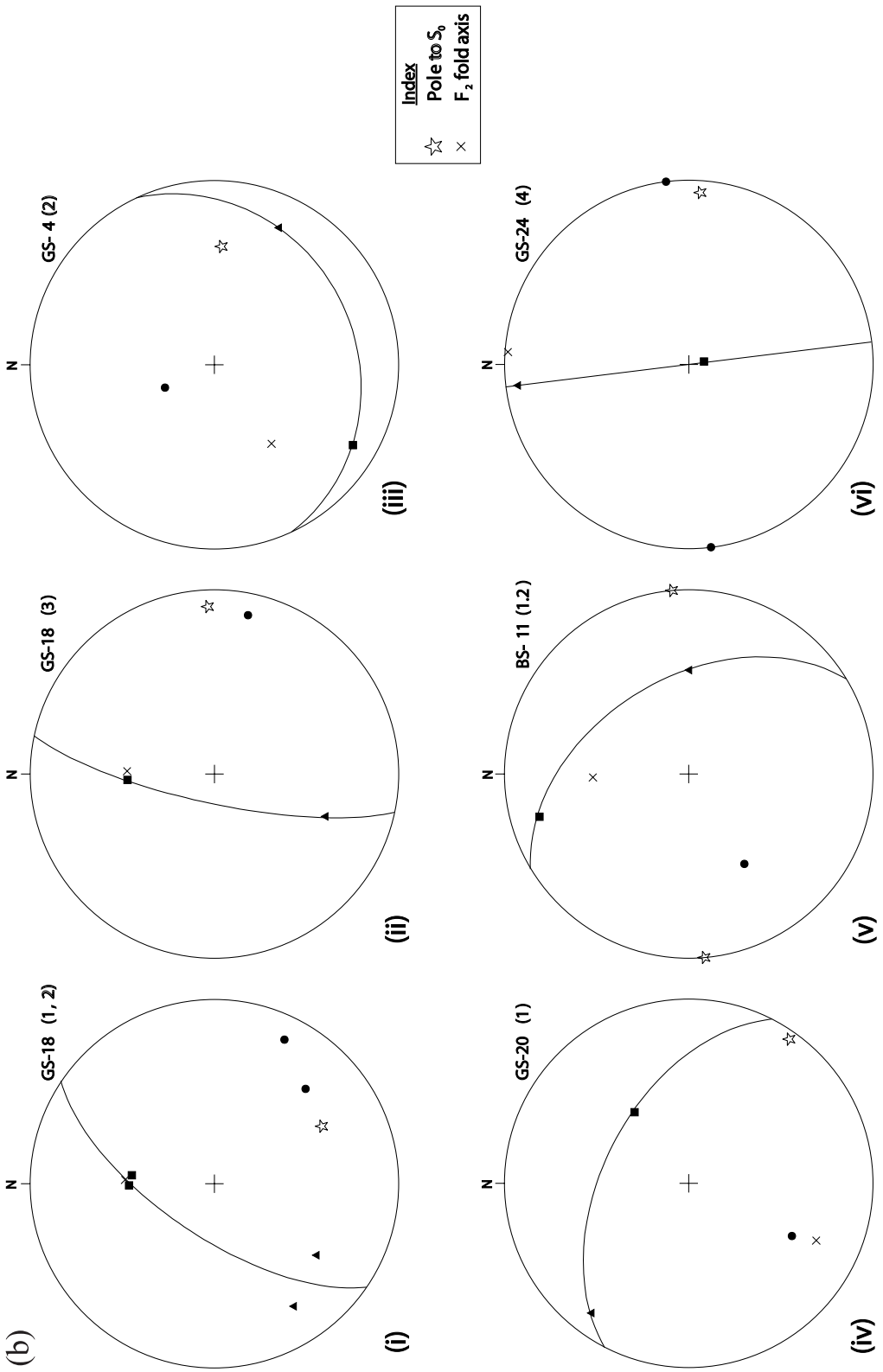

Fig. 5. Lower hemisphere equal-area projections of AMS directional data of samples collected from (a) limbs and (b) hinges of mesoscopic folds listed in Table 1. The magnetic foliation (F) is defined by the common great circle passing through K_1 (filled square) and K_2 (filled triangle). The pole to this F is K_3 (filled circle). The angle between K_3 and S_0 (shown by star) is very small for samples from limbs (a) but varies from moderate to high for samples from hinges (b) (see text for discussion). Sample numbers with the core specimen number (within brackets) are indicated at the top right of each stereogram.

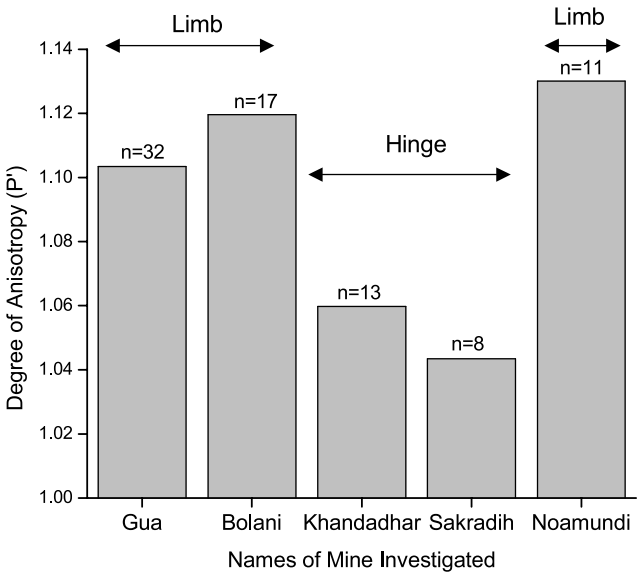

Fig. 6. Histogram comparing the degree of anisotropy (P') of samples from the limb and hinge portions of the Bonai Synclinorium.

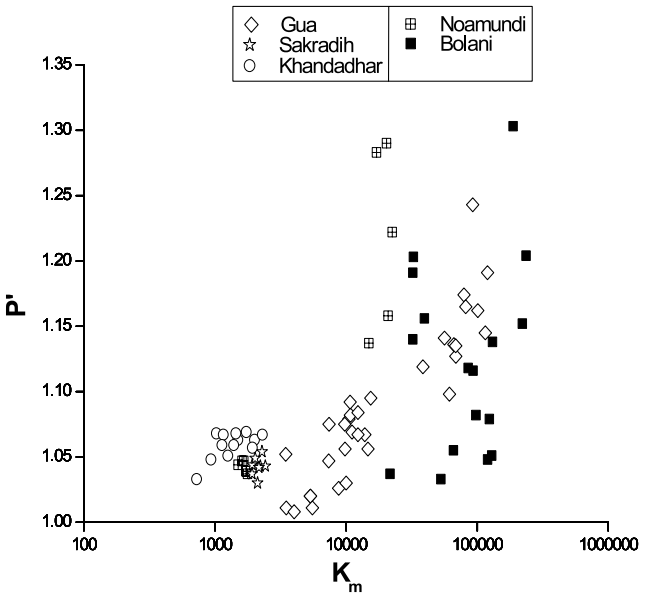

Fig. 7. Graph of degree of anisotropy (P') vs. mean bulk susceptibility (K_m) of the samples analysed from all the mines within the Bonai Synclinorium.

although the angle between the bedding plane and magnetic foliation in hinge parts of mesoscopic folds is moderate to high, the P' values are lower than those for limbs. However, the magnetic foliation in the hinge part is parallel to the axial plane direction of folds. Therefore, it is inferred that the magnetic fabric developed in the hinge part of folds is related to deformation. Microscopic evidence of ore minerals reoriented and recrystallised parallel to the axial planar direction has been noted in the hinge part of folds, which supports the above inference (Fig. 9). In samples from the limbs of folds, a parallelism between the bedding plane and magnetic foliation gives an apparent impression that the AMS fabric from the limbs is related to primary/sedimentary fabric rather than a tectonic/deformation event. A discussion about the mechanism of folding is essential to understand the above. It was stated earlier from structural analysis of field data that flexural folding is an important mechanism in the rocks of the study area. It is known that such a mechanism must result in Class-1B folds (Ramsay, 1967; Twiss and Moores, 1992). However, the geometry of folds in the study area is that of Class-1C, where the hinges are thicker than the limbs. Therefore, it is inferred that homogenous shortening along with flexural folding must have resulted in such geometry. It is envisaged that during such homogeneous shortening of a BIF, there would be a tendency for the already existing fabric in the limbs to be accentuated by further alignment and recrystallization of minerals in a direction that is at high angles to the shortening direction, ideally along the axial planar direction. However, since the rock is a BIF, the reorientation and recrystallization in the axial planar direction is more complete in the hinge part of the fold (Fig. 9), while in the limbs, the reorientation and recrystallization is limited/controlled by the orientation of the already existing fabric, i.e. bedding plane. In other words, in the limbs, the existing fabric (bedding plane) acts almost like a fabric-attractor (Passchier, 1997) and the minerals in the rock have a tendency to reorient/recrystallize in that direction. This results in a bedding-parallel tectonic fabric. The fact that the P' value for samples from limbs is higher than that from hinges also implies that if there was a sedimentary fabric, it was obliterated and totally superimposed by the tectonic fabric. Therefore, according to the authors, the parallelism between S_0 and magnetic foliation in Fig. 5a is because of a bedding-parallel tectonic fabric and not a sedimentary (bedding) fabric. Support for the limbs being strained also comes from microstructures like thinning and pinching of iron-ore rich bands in the limb parts of the small-scale folds. Thus, on the basis of the above evidence and arguments, it is concluded that the magnetic foliation in the Banded Iron Formations (BIFs) of the Singhbhum Orissa Iron Ore Craton in eastern India is related to ductile deformation and is tectonic in origin.

It was mentioned in Section 1 that strain analysis in rocks like BIFs is a challenge since they do not generally have any strain markers. Moreover, BIFs are lithologies that rarely develop mesoscopic foliations, except structures such as axial plane fractures that can be identified in the field. The present study highlights that despite the above inherent qualities of BIFs, AMS can be useful for strain analysis, identification of deformation fabrics and providing information that helps decipher the fold mechanism.

6. Conclusion

The present study exemplifies the application of AMS studies in analyses of deformed rocks. In rocks such as the

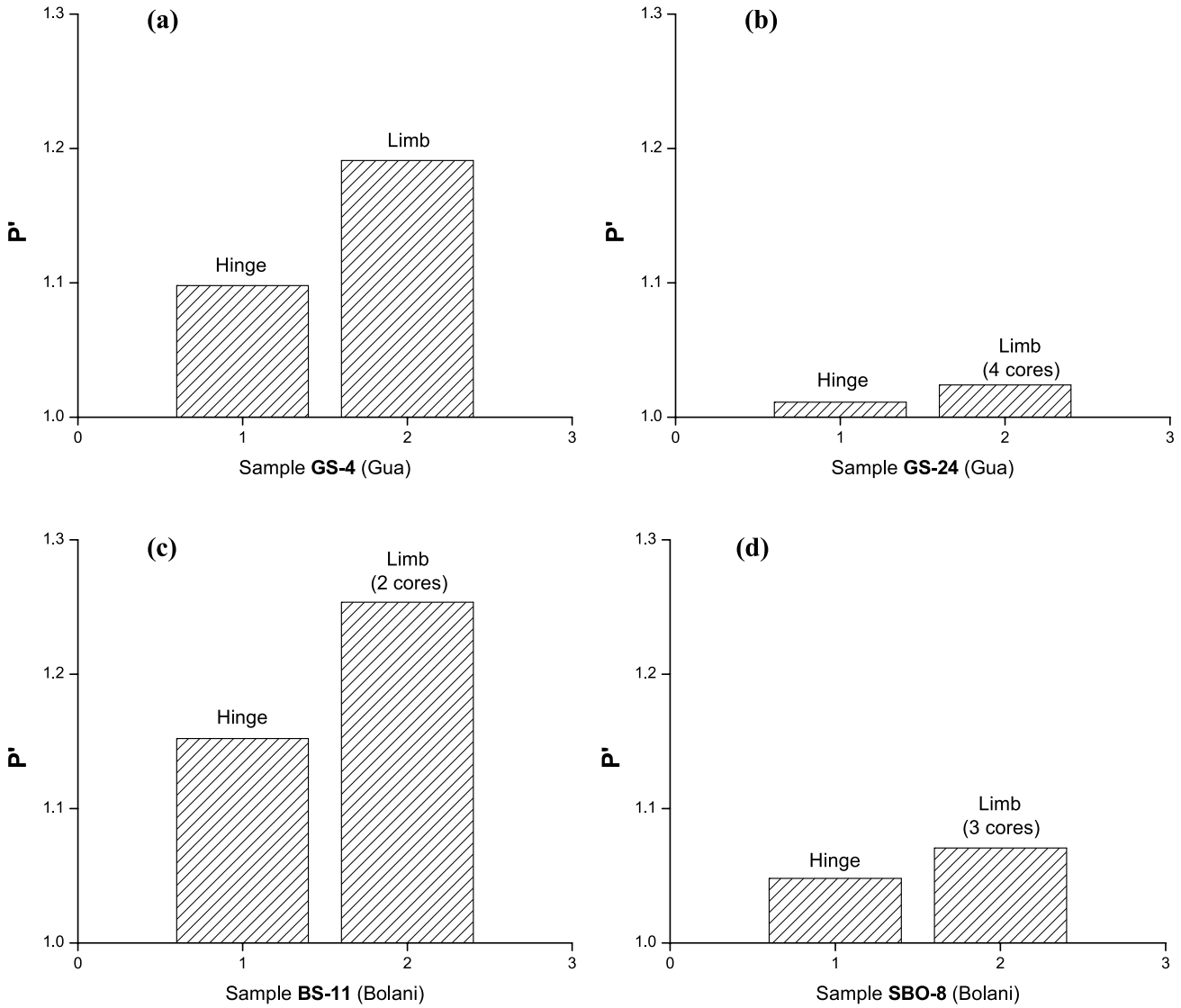

Fig. 8. Histograms showing the variation in P' values in samples from hinges and limbs of individual mesoscopic folds from Gua ((a) and (b)) and Bolani ((c) and (d)).

BIFs that have been investigated in the present case, there is no penetrative mesoscopic axial planar fabric. However, samples from the hinge of the folds have a magnetic foliation that lies at a moderate to high angle to the bedding plane. This implies that the fabric is tectonic in origin and that the magnetic data record the deformation imprint, although on the mesoscopic scale there was no axial plane foliation developed. Moreover, in the BIFs, strain analysis using the conventional methods is a challenge because of the absence of suitable strain markers. As a consequence, it is difficult to make comparisons of strain in different parts of a region or to note strain variations. The degree of magnetic anisotropy (P') determined from AMS studies is found to be useful for this purpose. Since the bulk susceptibility of a sample is controlled by the type and percentage of minerals (paramagnetic, diamagnetic and ferromagnetic) present in the rock, caution needs to be exercised when correlating P' with the absolute magnitude of strain. However, correlation between the P' values in rocks of similar lithology and comparable bulk susceptibility in different parts of a BIF can help in recognizing strain variations that would otherwise have gone unrecorded.

Acknowledgements

The authors are grateful to Helga de Wall for constructive suggestions on the AMS work on BIFs of eastern India that improved their understanding of the subject. However, the authors take full responsibility for the interpretations made in the present study. Thanks are due to Horst Quade and Anke Günther for discussions and to Satish

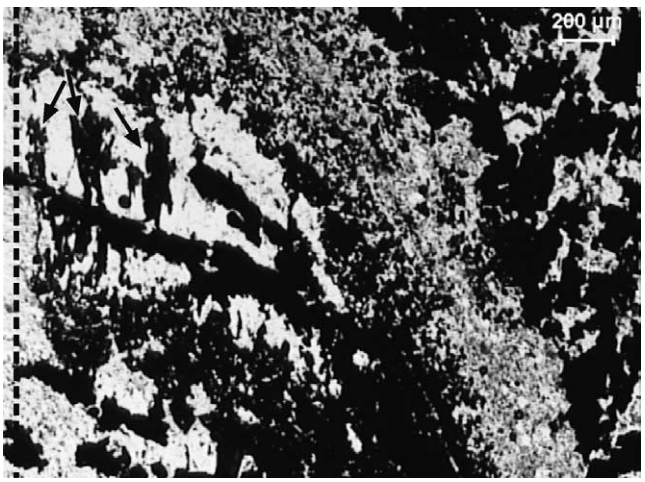

Fig. 9. Photomicrograph (in PPL) of a BIF sample showing a part of the hinge and limb of a fold. Note the presence of reoriented ore minerals (shown by arrows) parallel to the axial plane direction (shown by dashed line) at the hinge of the fold.

Sangode of Wadia Institute of Himalayan Geology (Dehradun, India) for extending facilities to carry out AMS analyses. Reviews by an anonymous referee and F. Hrouda helped improve the clarity of the paper. The study is a part of AM's doctoral research that was funded by the Institute Research Scholarship of the IIT, Kharagpur (India).

References

Archanjo, C.J., Bouchez, J.L., Corsini, M., Vauchez, A., 1994. The Pombal granite pluton: magnetic fabric, emplacement and relationships with the Brasiliano strike-slip setting of NE Brazil (Paraiba State). Journal of Structural Geology 16, 323–336.

Benn, K., Ham, N.M., Pignotta, G.S., 1998. Emplacement and deformation of granites during transpression: magnetic fabrics of the Archean Sparrow pluton, Slave Province, Canada. Journal of Structural Geology 20, 1247–1259.

Benn, K., Roest, W.R., Rochette, P., Evans, N.G., Pignotta, G.S., 1999. Geophysical and structural signatures of syntectonic batholith construction: the South Mountain Batholith, Meguma Terrane, Nova Scotia. Geophysics Journal International 136, 144–158.

Borradaile, G.J., 1988. Magnetic susceptibility, petrofabrics and strain. Tectonophysics 156, 1–20.

Borradaile, G.J., Alford, C., 1987. Relationship between magnetic susceptibility and strain in laboratory experiments. Tectonophysics 133, 121–135.

Borradaile, G.J., Henry, B., 1997. Tectonic applications of magnetic susceptibility and its anisotropy. Earth Science Reviews 42, 49–93.

Bouchez, J.L., 1997. Granite is never isotropic: an introduction to AMS studies of granitic rocks. In: Bouchez, J.L., Hutton, D.W.H., Stephens, W.E. (Eds.), Granite: From Segregation of Melt to Emplacement Fabrics, Kluwer, Dordrecht, The Netherlands, pp. 95–112.

Bouchez, J.L., Gleizes, G., Djouadi, T., Rochette, P., 1990. Microstructure and magnetic susceptibility applied to emplacement kinematics of granites: the example of the Foix pluton (French Pyrenees). Tectonophysics 184, 157–171.

Cruden, A.R., Launeau, P., 1994. Structure, magnetic fabric and emplacement of the Archean Lebel Stock, SW Abitibi Greenstone Belt. Journal of Structural Geology 16, 677–691.

Das, A.K., Piper, J.D.A., Mallik, S.B., Sherwood, G.J., 1996. Palaeomagnetic study of Archaean Banded Hematite Jasper Rocks from the Singhbhum–Orissa Craton, India. Precambrian Research 80, 193–204.

de Wall, H., Greiling, R.O., Sadek, M.F., 2001. Post-collisional shortening in the late Pan-African Hamisana high strain zone, SE Egypt: field and magnetic fabric evidence. Precambrian Research 107, 79–194.

Djouadi, M.T., Gleizes, G., Ferré, E., Bouchez, J.L., Caby, R., Lesquer, A., 1997. Oblique magmatic structures of two epizonal granite plutons, Hoggar, Algeria: late-orogenic emplacement in a transcurrent orogen. Tectonophysics 279, 351–374.

Ferré, E., Gleizes, G., Djouadi, M.T., Bouchez, J.-L., 1997. Drainage and emplacement of magmas along an inclined transcurrent shear zone: petrophysical evidence from a granite–charnockite pluton (Rahama, Nigeria). In: Bouchez, J.L., Hutton, D.W.H., Stephens, W.E. (Eds.), Granite: From Segregation of Melt to Emplacement Fabrics, Kluwer, Dordrecht, The Netherlands, pp. 253–273.

Ferré, E.C., Wilson, J., Gleizes, G., 1999. Magnetic susceptibility and AMS of the Bushveld Alkaline granites, South Africa. Tectonophysics 307, 113–133.

Ferré, E., Gleizes, G., Caby, R., 2002. Obliquely convergent tectonics and granite emplacement in the Trans-Saharan belt of Eastern Nigeria—a synthesis. Precambrian Research 114, 199–219.

Gleizes, G., Leblanc, D., Bouchez, J.-L., 1997. Variscan granites of the Pyrenees revisited: their role as syntectonic markers of the orogen. Terra Nova 9, 28–41.

Gleizes, G., Leblanc, D., Santana, V., Olivier, P., Bouchez, J.-L., 1998a. Sigmoidal structures featuring dextral shear during emplacement of the Hercynian granite complex of Cauterets–Panticosa (Pyrenees). Journal of Structural Geology 20, 1229–1245.

Gleizes, G., Leblanc, D., Bouchez, J.-L., 1998b. The main phase of the Hercynian orogeny in the Pyrenees is a dextral transpression. In: Holdsworth, R.E., Strachan, R.A., Dewey, J.F. (Eds.), Continental Transpressional and Transtensional Tectonics, Geological Society of London Special Publication, 135., pp. 267–273.

Gleizes, G., Leblanc, D., Oliver, P., Bouchez, J.-L., 2001. Strain partitioning in a pluton during emplacement in a transpressional regime: the example of the Neoville Granite (Pyrenees). International Journal of Earth Sciences 90, 325–340.

Greiling, R.O., Verma, P.K., 2001. Strike-slip tectonics and granitoid emplacement: an AMS fabric study from the Odenwald Crystalline Complex, SW Germany. Mineralogy and Petrology 72, 165–184.

Hrouda, F., 1978. The magnetic fabric in some folds. Physics of Earth and Planetary Interiors 17, 89–97.

Hrouda, F., 1993. Theoretical models of magnetic anisotropy to strain relationship revisited. Physics of the Earth and Planetary Interiors 77, 237–249.

Hrouda, F., Krejči, O., Otava, J., 2000. Magnetic fabrics in folds of the Eastern Rheno-Hercynian Zone. Physics and Chemistry of the Earth (A) 25, 505–510.

Hrouda, F., Putiš, M., Madarás, A., 2002. The Alpine overprints of the magnetic fabrics in the basement and cover rocks of the Veporic Unit (Western Carpathians, Slovakia). Tectonophysics 359, 271–288.

Jayangondaperumal, R., Dubey, A.K., 2001. Superposed folding of a blind thrust and formation of klippen: results of anisotropic magnetic susceptibility studies from the Lesser Himalaya. Journal of Asian Earth Sciences 19, 713–725.

Jones, H.C., 1934. The iron ores of Bihar and Orissa. Memoir of Geological Survey of India 63, 167–302.

Leblanc, D., Gleizes, G., Roux, L., Bouchez, J.L., 1996. Variscan dextral transpression in the French Pyrenees: new data from the Pic des Trois-Seigneurs granodiorite and its country rocks. Tectonophysics 261, 331–345.

Lister, G.S., Williams, P.F., 1983. The partitioning of deformation in flowing rock masses. In: Etheridge, M.A., Cox, S.F. (Eds.), Deformation Processes in Tectonics, Tectonophysics, 92., pp. 1–33.

Mallik, S.B., Sherwood, G.J., Das, A.K., 1993. The magnetic mineralogy of the Precambrian Banded Hematite Jasper Formation, Orissa, India. Journal of Geomagnetism and Geoelectricity 45, 155–165.

Mamtani, M.A., Greiling, R.O., Karanth, R.V., Merh, S.S., 1999. Orogenic deformation and its relationship to AMS fabric—an example from the southern margin of the Aravalli Mountain Belt, India. In: Radhakrishna, T., Piper, J.D. (Eds.), The Indian Subcontinent and Gondwana: a Palaeomagnetic and Rock Magnetic Perspective, Geological Society of India Memoir, 44., pp. 9–24.

Naha, K., Chaudhuri, A.K., 1968. Large-scale fold interference in a metamorphic–migmatitic complex. Tectonophysics 6, 127–142.

Neves, S.P., Araujo, A.M.B., Correia, P.B., Mariano, G., 2003. Magnetic fabrics in the Cabanas Granite (NE Brazil) Interplay between emplacement and regional fabrics in a dextral transpressive regime. Journal of Structural Geology 25, 441–453.

Passchier, C.W., 1997. The fabric attractor. Journal of Structural Geology 19, 113–127.

Ramsay, J.G., 1967. Folding and Fracturing of Rocks, McGraw-Hill Book Company, New York.

Ramsay, J.G., Huber, M.I., 1983. The Techniques of Modern Structural Geology. Volume-I: Strain Analysis, Academic Press, London.

Rathore, J.S., 1979. Magnetic susceptibility anisotropy in the Cambrian Slate Belt of North Wales and correlation with strain. Tectonophysics 53, 83–97.

Rathore, J.S., Henry, B., 1982. Comparison of strain and magnetic fabrics in Dalradian rocks from the southwest Highlands of Scotland. Journal of Structural Geology 4, 373–384.

Saha, A.K., 1994. Crustal Evolution of Singhbhum North Orissa Province, Eastern India. Memoir-27, Geological Society of India, Bangalore.

Saha, A.K., Ray, S.L., Sarkar, S.N., 1988. Early history of the Earth: evidence from the Eastern Indian shield. In: Mukhopadhyay, D., (Ed.), Precambrian of the Eastern Indian Shield, Memoir of Geological Society of India, 8., pp. 13–37.

Saint-Blanquat, M., Tikoff, B., 1997. Development of magmatic to solid-state fabrics during syntectonic emplacement of the Mona Creek granite, Sierra Nevada Batholith, California. In: Bouchez, J.L., Hutton, D.W.H., Stephens, W.E. (Eds.), Granite: From Segregation of Melt to Emplacement Fabrics, Kluwer, Dordrecht, The Netherlands, pp. 231–252.

Siegesmund, S., Becker, J.K., 2000. Emplacement of Ardara pluton (Ireland): new constraints from magnetic fabrics, rock fabrics and age dating. International Journal of Earth Sciences 98, 307–327.

Tarling, D.H., Hrouda, F., 1993. The Magnetic Anisotropy of Rocks, Chapman and Hall, London.

Tomezzoli, R.N., Macdonald, W.D., Tickyj, H., 2003. Composite magnetic fabrics and S–C structure in granite gneiss of Cerro de lo Viejos, La Pampas province, Argentina. Journal of Structural Geology 25, 159–169.

Twiss, R.J., Moores, E.M., 1992. Structural Geology, Freeman and Company, New York.